Inverse problem in optical diffusion tomography. III. Inversion formulas and singular-value decomposition

Vadim A. Markel

Department of Radiology, Washington University, St. Louis, Missouri 63110

Vivek Mital

Department of Electrical Engineering, Washington University, St. Louis, Missouri 63130

John C. Schotland*

Departments of Electrical Engineering and Radiology, Washington University, St. Louis, Missouri 63130

Received June 19, 2002; revised manuscript received November 11, 2002; accepted December 4, 2002

We continue our study of the inverse scattering problem for diffuse light. In particular, we derive inversion formulas for this problem that are based on the functional singular-value decomposition of the linearized forward-scattering operator in the slab, cylindrical, and spherical geometries. Computer simulations are used to illustrate our results in model systems. © 2003 Optical Society of America

OCIS codes: 170.0170, 170.3010, 170.3660, 170.6960.

1. INTRODUCTION

This paper is the third in a series devoted to the inverse scattering problem (ISP) for diffuse light. The study of this problem is of fundamental importance for the development of image reconstruction algorithms in optical diffusion tomography. For a sample of the current activity in this field, see, for example, Refs. 1 and 2; a more detailed review of the relevant literature has been given in Ref. 3. Here we only note that the standard approach to image reconstruction is based on numerical methods that involve, either explicitly or implicitly, minimization of certain functionals.[4] Although this approach is extremely flexible and allows for the consideration of scattering media with arbitrarily shaped boundaries, it is inefficient computationally, particularly when a large number of source–detector pairs is employed for three-dimensional imaging. In Refs. 3 and 5, we have developed the scattering theory of diffusing waves in inhomogeneous media and investigated the mathematical structure of the linearized ISP. In this paper we exploit these results to obtain a general class of inversion formulas for the ISP that are based on the singular-value decomposition (SVD) of the linearized forward-scattering operator. The inversion formulas rely on the existence of certain symmetries of the surface of the scattering medium and lead to computationally efficient and numerically stable reconstruction algorithms. We have previously reported inversion formulas in the planar geometry with free boundaries[6] and for the case of arbitrary boundary conditions.[7] In the present work we give a detailed derivation of the inversion formulas and generalize them to the cylindrical and spherical geometries. Numerical reconstructions are performed in the planar and cylindrical cases. We consider the linearized ISP within the first Born approximation; generalization to the nonlinear ISP will be discussed in the fourth paper of this series.

We begin by recalling the relevant mathematical formalism. We assume that the energy density $u(\mathbf{r}, t)$ of diffuse light in an inhomogeneous medium obeys the diffusion equation

$$\frac{\partial u(\mathbf{r}, t)}{\partial t} = \nabla \cdot [D(\mathbf{r})\nabla u(\mathbf{r}, t)] - \alpha(\mathbf{r})u(\mathbf{r}, t) + S(\mathbf{r}, t). \tag{1}$$

Here $\alpha(\mathbf{r})$ and $D(\mathbf{r})$ are the position-dependent absorption and diffusion coefficients, and $S(\mathbf{r}, t)$ is the power density of the source. Note that α and D are related to the absorption and reduced-scattering coefficients μ_a and μ_s', which appear in the radiative transport equation, by $\alpha = c\mu_a$ and $D = c/3(\mu_a + \mu_s')$, where c is the speed of light in the medium. We further assume that the source is harmonically modulated with frequency ω. In addition to Eq. (1), the energy density must satisfy boundary conditions on the surface of the medium (or at infinity in the case of free boundaries). In general, we will consider boundary conditions of the form

$$u + l\hat{\mathbf{n}} \cdot \nabla u = 0, \tag{2}$$

where l is the extrapolation length.[8] Note that we obtain purely absorbing boundaries in the limit $l = 0$ and purely reflecting boundaries in the limit $l \to \infty$.

As shown in Papers I and II of this series, the diffusion equation (1) may be solved with the use of an appropriate Green's function. The Green's function may be directly

 © 2003 Optical Society of America

related to the intensity measured by a point detector when the medium is illuminated by a point source. In the first Born approximation, the change in intensity of transmitted light (at the modulation frequency) due to spatial fluctuations in $\alpha(\mathbf{r})$ and $D(\mathbf{r})$ is given by the integral equation[5]

$$\phi(\mathbf{r}_1, \mathbf{r}_2) = \beta \int G_0(\mathbf{r}_1, \mathbf{r}) V(\mathbf{r}) G_0(\mathbf{r}, \mathbf{r}_2) \mathrm{d}^3 r. \quad (3)$$

Here the data function $\phi(\mathbf{r}_1, \mathbf{r}_2)$ is proportional to the change in complex intensity relative to a reference medium with absorption α_0 and diffusion constant D_0, $\delta\alpha(\mathbf{r}) = \alpha(\mathbf{r}) - \alpha_0$, $\delta D(\mathbf{r}) = D(\mathbf{r}) - D_0$, and $\mathbf{r}_1$ and $\mathbf{r}_2$ denote the coordinates of the source and the detector, respectively. We have also found it useful to introduce the notation

$$V(\mathbf{r}) \equiv \delta\alpha(\mathbf{r}) - \nabla \cdot \delta D(\mathbf{r}) \nabla, \quad (4)$$

$$\beta = \begin{cases} 1 & \text{for free boundaries} \\ (1 + \ell^*/\ell)^2 & \text{for boundary conditions, of the type (2)} \end{cases} \quad (5)$$

where $\ell^* = 3D_0/c$. The unperturbed Green's function $G_0(\mathbf{r}, \mathbf{r}')$ satisfies

$$(\nabla^2 - k^2) G_0(\mathbf{r}, \mathbf{r}') = -\frac{1}{D_0} \delta(\mathbf{r} - \mathbf{r}'), \quad (6)$$

where the diffuse wave number k is given by

$$k^2 = \frac{\alpha_0 - i\omega}{D_0} \quad (7)$$

and $G_0(\mathbf{r}, \mathbf{r}')$ satisfies the boundary condition (2).

Equation (3) is the main integral equation that will be inverted in this paper. The approach that we will follow involves constructing the SVD of the integral operator defined by Eq. (3). The SVD provides a precise characterization of the ISP and may be used to derive an inversion formula that leads to a computationally efficient and numerically stable algorithm. We have previously described SVD inversion formulas for the cases of the planar measurement geometry with free boundaries[6] and for boundary conditions of the form (2).[7] In this paper we generalize the results of Refs. 6 and 7 to the cylindrical and spherical geometries and present important calculational details for the planar geometry. We also implement the SVD inversion formula in the cylindrical geometry and present reconstructions of the absorption and diffusion coefficients using two modulation frequencies.

The remainder of this paper is organized as follows. Section 2 contains a derivation of an SVD inversion formula for discretized one-dimensional integral equations, a mathematical tool that is used in subsequent sections. In Sections 3, 4, and 5, we derive inversion formulas for the planar, cylindrical, and spherical measurement geometries, respectively. Finally, Section 7 describes simulated reconstructions in the cylindrical geometry.

2. SINGULAR-VALUE DECOMPOSITION FOR ONE-DIMENSIONAL INTEGRAL EQUATIONS

The ISP consists in reconstructing $\delta\alpha(\mathbf{r})$ and $\delta D(\mathbf{r})$ from the data function $\phi(\mathbf{r}_1, \mathbf{r}_2)$. To this end we will construct the pseudoinverse solution to the integral equation (3). In this section we consider an intermediate step in the calculation, namely, the SVD for one-dimensional integral equations with discrete data. We begin by briefly reviewing the SVD of linear operators on Hilbert spaces.[9]

A. Singular-Value Decomposition

Let A denote a linear integral operator with the kernel $A(x, y)$ that maps the Hilbert space $\mathcal{H}_1$ into the Hilbert space $\mathcal{H}_2$. By the SVD of A, we mean a representation of the form

$$A(x, y) = \sum_n \sigma_n g_n(x) f_n^*(y), \quad (8)$$

where σ_n is the singular value associated with the singular functions f_n and g_n. The $\{f_n\}$ and the $\{g_n\}$ are orthonormal bases of $\mathcal{H}_1$ and $\mathcal{H}_2$, respectively, and are eigenfunctions with eigenvalues σ_n^2 of A^*A and AA^*:

$$A^*A f_n = \sigma_n^2 f_n, \quad (9)$$

$$AA^* g_n = \sigma_n^2 g_n. \quad (10)$$

In addition, the f_n and the g_n are related by

$$A f_n = \sigma_n g_n, \quad (11)$$

$$A^* g_n = \sigma_n f_n. \quad (12)$$

The pseudoinverse solution to the equation $Af = g$ is defined to be the minimizer of $\|Af - g\|$ with smallest norm. This well-defined element $f^+ \in [N(A)]^\perp$ is unique and may be shown[9] to be of the form $f^+ = A^+ g$, where the pseudoinverse operator A^+ is given by $A^+ = A^*(AA^*)^{-1}$ and $[N(A)]^\perp$ denotes the orthogonal complement of the null space of A. The SVD of A may be used to express A^+ as

$$A^+(x, y) = \sum_n \frac{1}{\sigma_n} f_n(x) g_n^*(y). \quad (13)$$

B. One-Dimensional Integral Equations

Consider the set of N one-dimensional integral equations of the form

$$\int_0^L K_n(z) f(z) \mathrm{d}z = F_n, \qquad n = 1, \ldots, N. \quad (14)$$

The functions $K_n(z)$ define a linear operator K that maps $L^2([0, L])$ into $\mathbb{C}^N$. Using the above results, we may see that the SVD of K is given by

$$K_n(z) = \sum_l \sigma_l (g_l)_n f_l^*(z). \quad (15)$$

Here the singular vectors g_l are eigenvectors of $M = KK^*$ with eigenvalue σ_l^2, that is, $Mg_l = \sigma_l^2 g_l$. The

matrix elements of M, which is an $N \times N$ positive-definite matrix, are given by

$$M_{mn} = \int_0^L K_m(z) K_n^*(z) \mathrm{d}z. \tag{16}$$

The singular functions $f_l(z)$ are given by $f_l = K^* g_l$, or, more explicitly,

$$f_l(z) = \frac{1}{\sigma_l} \sum_n K_n^*(z) (g_l)_n. \tag{17}$$

The SVD of K may be used to obtain the pseudoinverse operator K^+, which is given by the expression

$$K_n^+(z) = \sum_l \frac{1}{\sigma_l} (g_l^*)_n f_l(z). \tag{18}$$

Using Eq. (17) and the spectral decomposition for M^{-1}, given by

$$M_{mn}^{-1} = \sum_l \frac{1}{\sigma_l^2} (g_l)_m (g_l^*)_n, \tag{19}$$

we may rewrite Eq. (18) as

$$K_n^+(z) = \sum_m K_m^*(z) M_{mn}^{-1}. \tag{20}$$

Thus the pseudoinverse solution to Eq. (14) is given by

$$f(z) = \sum_{m,n} K_m^*(z) M_{mn}^{-1} F_n. \tag{21}$$

Note that some of the eigenvalues of M can vanish or be extremely small. The pseudoinverse solution (21) must then be *regularized*. This can be achieved, for example, by setting

$$M_{mn}^{-1} = \sum_l \Theta(\sigma_l - \epsilon) \frac{1}{\sigma_l^2} (g_l)_m (g_l^*)_n, \tag{22}$$

where $\Theta(x)$ is the step function and ϵ is a small parameter.

As an example, consider the case $K_n(z) = \exp(ip_n z)$, where all discrete values p_n are multiples of $2\pi/L$. In this case Eq. (14) defines a discrete Fourier transform. It can be easily seen that $M_{mn} = L\delta_{mn}$ and $M_{mn}^{-1} = L^{-1}\delta_{mn}$. Therefore the pseudoinverse solution (21) is equivalent to the inverse Fourier transform:

$$f(z) = L^{-1} \sum_{n=1}^{N} \exp(-ip_n z) F_n. \tag{23}$$

In the case of the discrete Laplace transform $[K_n(z) = \exp(-p_n z)]$, the matrix M is more complicated: For purely real p_n's, $M_{mn} = \{1 - \exp[-(p_m + p_n)L]\}/(p_m + p_n)$. As N increases, the determinant of this matrix becomes very small. This reflects the ill posedness of the Laplace transform inversion. In this case the pseudoinverse solution must be regularized according to Eq. (22).

Finally, we generalize our results for the case of a one-dimensional integral equation that contains several unknown functions and, correspondingly, several different kernels:

$$\int_0^L \sum_{p=1}^{P} K_n^{(p)}(z) f^{(p)}(z) \mathrm{d}z = F_n, \qquad n = 1,\ldots,N. \tag{24}$$

Following the arguments outlined above, the pseudoinverse solution is given by

$$f^{(p)}(z) = \sum_{m,n} K_m^{(p)*}(z) M_{mn}^{-1} F_n, \tag{25}$$

where

$$M_{mn} = \int_0^L \sum_{p=1}^{P} K_m^{(p)}(z) K_n^{(p)*}(z) \mathrm{d}z. \tag{26}$$

3. PLANAR GEOMETRY

We begin the study of the ISP in the planar geometry, since this is the simplest case to consider. The solution to the inverse problem with measurements taken on a single plane with free boundaries was described in Ref. 6. However, the derivations in Ref. 6 are based on a direct calculation of the singular functions and are rather complex. Here we present a simplified derivation and generalize the results to the case of two measurement planes and boundary conditions of the form (2). An account of the ISP in the slab geometry was also presented in Ref. 7 but with few mathematical details.

A. Single Plane

Consider the physical situation when both sources and detectors are located on the plane $z = 0$ and all inhomogeneities are confined to the region $0 < z < L$. The limit $L \to \infty$ can be considered a special case. In this geometry the unperturbed Green's function can be written as

$$G_0(\mathbf{r}, \mathbf{r}') = \int \frac{\mathrm{d}^2 q}{(2\pi)^2} g(\mathbf{q}; z, z') \exp[i\mathbf{q} \cdot (\boldsymbol{\rho}' - \boldsymbol{\rho})]. \tag{27}$$

Here $\mathbf{q}$ is a two-dimensional vector parallel to the plane $z = 0$, and we have used the notation $\mathbf{r} = (\boldsymbol{\rho}, z)$. The function $g(\mathbf{q}; z, z')$ is given in the case of free boundaries by[3]

$$g(\mathbf{q}; z, z') = \frac{\exp[-Q(\mathbf{q})|z - z'|]}{2Q(\mathbf{q})D_0} \tag{28}$$

and in the case of boundary conditions of the type (2) by[5]

$$g(\mathbf{q}; z, z') = \frac{1}{2Q(\mathbf{q})D_0} \left\{ \exp[-Q(\mathbf{q})|z - z'|] + \frac{Q(\mathbf{q})l - 1}{Q(\mathbf{q})l + 1} \exp[-Q(\mathbf{q})|z + z'|] \right\}, \tag{29}$$

where

$$Q(\mathbf{q}) \equiv \sqrt{\mathbf{q}^2 + k^2}. \tag{30}$$

The definition of the data function (3) contains only Green's functions with $\mathbf{r}_1$ or $\mathbf{r}_2$ on the boundary surface.

7In this case we can simplify Eqs. (28) and (29) by setting z' or z to zero. Then the expression for g becomes

$$g(\mathbf{q};\, z,\, 0) = g(\mathbf{q};\, 0, z) = \tilde{g}(\mathbf{q};\, z), \tag{31}$$

where

$$\tilde{g}(\mathbf{q};\, z) = \frac{\exp[-Q(\mathbf{q})|z|]}{2D_0 Q(\mathbf{q})} \qquad \text{(free boundaries)}, \tag{32}$$

$$\tilde{g}(\mathbf{q};\, z) = \frac{l}{D_0}\frac{\exp[-Q(\mathbf{q})|z|]}{Q(\mathbf{q})l + 1} \qquad \text{(boundary conditions)}. \tag{33}$$

We now use the definition (3) to construct the data function $\phi(\boldsymbol{\rho}_1,\, \boldsymbol{\rho}_2)$, where the two-dimensional vectors $\boldsymbol{\rho}_1$ and $\boldsymbol{\rho}_2$ denote the locations of the sources and the detectors, respectively, on the measurement surface $z = 0$:

$$\begin{aligned}\phi(\boldsymbol{\rho}_1,\, \boldsymbol{\rho}_2) = \beta \int \frac{\mathrm{d}^2 q_1 \mathrm{d}^2 q_2}{(2\pi)^4} \int_{z>0} \mathrm{d}^3 r \tilde{g}(\mathbf{q}_1;\, z) \\ \times \exp[i\mathbf{q}_1 \cdot (\boldsymbol{\rho} - \boldsymbol{\rho}_1)] V(\mathbf{r}) \tilde{g}(\mathbf{q}_2;\, z) \\ \times \exp[i\mathbf{q}_2 \cdot (\boldsymbol{\rho}_2 - \boldsymbol{\rho})].\end{aligned} \tag{34}$$

Next, we Fourier-transform the data function with respect to the two-dimensional variables $\boldsymbol{\rho}_1$ and $\boldsymbol{\rho}_2$ according to

$$\begin{aligned}\phi(\mathbf{q}_1,\, \mathbf{q}_2) = \int \mathrm{d}^2\rho_1 \mathrm{d}^2\rho_2 \phi(\boldsymbol{\rho}_1,\, \boldsymbol{\rho}_2) \\ \times \exp[i(\mathbf{q}_1 \cdot \boldsymbol{\rho}_1 + \mathbf{q}_2 \cdot \boldsymbol{\rho}_2)]\end{aligned} \tag{35}$$

and obtain

$$\begin{aligned}\phi(\mathbf{q}_1,\, \mathbf{q}_2) = \beta \int \mathrm{d}^3 r \tilde{g}(\mathbf{q}_1;\, z) \exp(i\mathbf{q}_1 \cdot \boldsymbol{\rho}) \\ \times V(\mathbf{r}) \tilde{g}(\mathbf{q}_2;\, z) \exp(i\mathbf{q}_2 \cdot \boldsymbol{\rho}).\end{aligned} \tag{36}$$

Now we use the definition of $V(\mathbf{r})$ [Eq. (4)] to rewrite the integral equation (36) in terms of the unknown functions $\delta\alpha(\mathbf{r})$ and $\delta D(\mathbf{r})$. Thus we have

$$\begin{aligned}\phi(\mathbf{q}_1,\, \mathbf{q}_2) = \int \mathrm{d}^3 r [\kappa_A(\mathbf{q}_1,\, \mathbf{q}_2;\, z)\delta\alpha(\mathbf{r}) \\ + \kappa_D(\mathbf{q}_1,\, \mathbf{q}_2;\, z)\delta D(\mathbf{r})] \exp[i(\mathbf{q}_1 + \mathbf{q}_2) \cdot \boldsymbol{\rho}],\end{aligned} \tag{37}$$

where

$$\kappa_A(\mathbf{q}_1,\, \mathbf{q}_2;\, z) = \beta \tilde{g}(\mathbf{q}_1;\, z) \tilde{g}(\mathbf{q}_2;\, z), \tag{38}$$

$$\begin{aligned}\kappa_D(\mathbf{q}_1,\, \mathbf{q}_2;\, z) = \beta \Bigg[\frac{\partial \tilde{g}(\mathbf{q}_1;\, z)}{\partial z} \frac{\partial \tilde{g}(\mathbf{q}_2;\, z)}{\partial z} \\ - \mathbf{q}_1 \cdot \mathbf{q}_2 \tilde{g}(\mathbf{q}_1;\, z) \tilde{g}(\mathbf{q}_2;\, z) \Bigg].\end{aligned} \tag{39}$$

Let us introduce the change of variables $\mathbf{q}_1 = \mathbf{q}/2 + \mathbf{p}_n$ and $\mathbf{q}_2 = \mathbf{q}/2 - \mathbf{p}_n$, where $\mathbf{q}$ is continuous and $\mathbf{p}_n\, (n = 1,...,N)$ is an arbitrary set of discrete vectors. Note that it may be expected that the accuracy of the solution to the ISP should improve when $N \to \infty$ and the $\mathbf{p}_n$'s span the two-dimensional space of wave vectors, thus taking into account all values of the four-dimensional data function $\phi(\mathbf{q}/2 + \mathbf{p}_n,\, \mathbf{q}/2 - \mathbf{p}_n)$. However, the ill posedness of the inverse problem constrains the set of "useful" vectors $\mathbf{p}_n$. The specific choice of this set is discussed in Section 6. We can then bring Eq. (37) to the following form:

$$F_n(\mathbf{q}) = \int_0^L \mathrm{d}z [K_n^{(A)}(\mathbf{q};\, z)a(\mathbf{q};\, z) + K_n^{(D)}(\mathbf{q};\, z)b(\mathbf{q};\, z)], \tag{40}$$

where

$$\begin{aligned}a(\mathbf{q};\, z) = \int \mathrm{d}^2\rho \delta\alpha(\mathbf{r}) \exp(i\mathbf{q} \cdot \boldsymbol{\rho}), \\ b(\mathbf{q};\, z) = \int \mathrm{d}^2\rho \delta D(\mathbf{r}) \exp(i\mathbf{q} \cdot \boldsymbol{\rho}),\end{aligned} \tag{41}$$

$$\begin{aligned}K_n^{(A)}(\mathbf{q};\, z) = \kappa_A(\mathbf{q}/2 + \mathbf{p}_n,\, \mathbf{q}/2 - \mathbf{p}_n;\, z), \\ K_n^{(D)}(\mathbf{q};\, z) = \kappa_D(\mathbf{q}/2 + \mathbf{p}_n,\, \mathbf{q}/2 - \mathbf{p}_n;\, z),\end{aligned} \tag{42}$$

$$F_n(\mathbf{q}) = \phi(\mathbf{q}/2 + \mathbf{p}_n,\, \mathbf{q}/2 - \mathbf{p}_n). \tag{43}$$

For fixed $\mathbf{q}$, Eq. (40) is in the form of the one-dimensional integral equation (24) with two unknown functions. Therefore it can be solved for $a(\mathbf{q};\, z)$ and $b(\mathbf{q};\, z)$ according to

$$a(\mathbf{q};\, z) = \sum_{m,n} K_m^{(A)*}(\mathbf{q};\, z) M_{mn}^{-1}(\mathbf{q}) F_n(\mathbf{q}), \tag{44}$$

$$b(\mathbf{q};\, z) = \sum_{m,n} K_m^{(D)*}(\mathbf{q};\, z) M_{mn}^{-1}(\mathbf{q}) F_n(\mathbf{q}), \tag{45}$$

$$\begin{aligned}M_{mn}(\mathbf{q}) = \int_0^L [K_m^{(A)}(\mathbf{q};\, z) K_n^{(A)*}(\mathbf{q};\, z) \\ + K_m^{(D)}(\mathbf{q};\, z) K_n^{(D)*}(\mathbf{q};\, z)] \mathrm{d}z.\end{aligned} \tag{46}$$

The functions $a(\mathbf{q};\, z)$ and $b(\mathbf{q};\, z)$ are related to the unknowns $\delta\alpha(\mathbf{r})$ and $\delta D(\mathbf{r})$ by the two-dimensional Fourier transforms (41), which can be easily inverted. Therefore we obtain

$$\begin{aligned}\delta\alpha(\mathbf{r}) = \int \frac{\mathrm{d}^2 q}{(2\pi)^2} \exp(-i\mathbf{q} \cdot \boldsymbol{\rho}) \\ \times \sum_{ml} K_m^{(A)*}(\mathbf{q};\, z) M_{ml}^{-1}(\mathbf{q}) F_l(\mathbf{q}),\end{aligned} \tag{47}$$

$$\begin{aligned}\delta D(\mathbf{r}) = \int \frac{\mathrm{d}^2 q}{(2\pi)^2} \exp(-i\mathbf{q} \cdot \boldsymbol{\rho}) \\ \times \sum_{ml} K_m^{(D)*}(\mathbf{q};\, z) M_{ml}^{-1}(\mathbf{q}) F_l(\mathbf{q}).\end{aligned} \tag{48}$$

Restoring the original notation, we obtain the inversion formulas

$$\tilde{g}(\mathbf{q};\, z,\, z') = \frac{\exp[-Q(\mathbf{q})|z - z'|]}{2D_0 Q(\mathbf{q})} \qquad \text{(free boundaries)}, \quad (54)$$

$$\tilde{g}(\mathbf{q};\, z,\, z') = \frac{l}{D_0}\frac{\sinh[Q(\mathbf{q})(L - |z - z'|)] + Q(\mathbf{q})l\cosh[Q(\mathbf{q})(L - |z - z'|)]}{\sinh[Q(\mathbf{q})L] + 2Q(\mathbf{q})l\cosh[Q(\mathbf{q})L] + [Q(\mathbf{q})l]^2\sinh[Q(\mathbf{q})L]} \qquad \text{(boundary conditions)}. \quad (55)$$

$$\delta\alpha(\mathbf{r}) = \int \frac{\mathrm{d}^2 q}{(2\pi)^2}\exp(-i\mathbf{q}\cdot\boldsymbol{\rho}) \times \sum_{m,n}\kappa_A^*\left(\frac{\mathbf{q}}{2} + \mathbf{p}_m,\, \frac{\mathbf{q}}{2} - \mathbf{p}_m;\, z\right) \times M_{mn}^{-1}(\mathbf{q})\phi\left(\frac{\mathbf{q}}{2} + \mathbf{p}_n,\, \frac{\mathbf{q}}{2} - \mathbf{p}_n\right), \quad (49)$$

$$\delta D(\mathbf{r}) = \int \frac{\mathrm{d}^2 q}{(2\pi)^2}\exp(-i\mathbf{q}\cdot\boldsymbol{\rho}) \times \sum_{m,n}\kappa_D^*\left(\frac{\mathbf{q}}{2} + \mathbf{p}_m,\, \frac{\mathbf{q}}{2} - \mathbf{p}_m;\, z\right) \times M_{mn}^{-1}(\mathbf{q})\phi\left(\frac{\mathbf{q}}{2} + \mathbf{p}_n,\, \frac{\mathbf{q}}{2} - \mathbf{p}_n\right), \quad (50)$$

$$M_{mn}(\mathbf{q}) = \int_0^L \Bigg[\kappa_A\left(\frac{\mathbf{q}}{2} + \mathbf{p}_m,\, \frac{\mathbf{q}}{2} - \mathbf{p}_m;\, z\right) \times \kappa_A^*\left(\frac{\mathbf{q}}{2} + \mathbf{p}_n,\, \frac{\mathbf{q}}{2} - \mathbf{p}_n;\, z\right) + \kappa_D\left(\frac{\mathbf{q}}{2} + \mathbf{p}_m,\, \frac{\mathbf{q}}{2} - \mathbf{p}_m;\, z\right) \times \kappa_D^*\left(\frac{\mathbf{q}}{2} + \mathbf{p}_n,\, \frac{\mathbf{q}}{2} - \mathbf{p}_n;\, z\right)\Bigg]\mathrm{d}z. \quad (51)$$

B. Two Planes

We now consider the case of measurements taken on two parallel planes $z = 0$ and $z = L$. The medium to be imaged is located between the planes in the region $0 < z < L$. The unperturbed Green's function in this case is given by Eq. (27) with

$$g(\mathbf{q};\, z,\, z') = \frac{l}{D_0}\frac{[1 + (Ql)^2]\cosh[Q(L - |z - z'|)] - [1 - (Ql)^2]\cosh[Q(L - |z + z'|)] + 2Ql\sinh[Q(L - |z - z'|)]}{2D_0 Q[\sinh(QL) + 2Ql\cosh(QL) + (Ql)^2\sinh(QL)]} \quad (52)$$

for boundary conditions of the form (2) and by Eq. (28) for free boundaries. The Green's functions that enter the definition of the data function simplify on the measurement surface, which allows us to write

$$g(\mathbf{q};\, z,\, z')|_{z'=0,L} = g(\mathbf{q};\, z',\, z)|_{z'=0,L} = \tilde{g}(q;\, z,\, z'), \quad (53)$$

where

Following the same procedure as that in Subsection 3.A, we arrive at an integral equation of the form (37), where the functions κ_A and κ_D are now given by

$$\kappa_A(\mathbf{q}_1,\, \mathbf{q}_2;\, z) = \beta\tilde{g}(\mathbf{q}_1;\, z_1,\, z)\tilde{g}(\mathbf{q}_2;\, z,\, z_2), \quad (56)$$

$$\kappa_D(\mathbf{q}_1,\, \mathbf{q}_2;\, z) = \beta\Bigg[\frac{\partial\tilde{g}(\mathbf{q}_1;\, z_1,\, z)}{\partial z}\frac{\partial\tilde{g}(\mathbf{q}_2;\, z,\, z_2)}{\partial z} - \mathbf{q}_1\cdot\mathbf{q}_2\tilde{g}(\mathbf{q}_1;\, z_1,\, z)\tilde{g}(\mathbf{q}_2;\, z,\, z_2)\Bigg]. \quad (57)$$

Here we have assumed that the sources and the detectors are located on the planes $z = z_1$ and $z = z_2$, respectively. Finally, given the expressions for κ_A and κ_D, the inversion formulas (49)–(51) can be applied.

C. Singular-Value-Decomposition Structure of the Inversion Formulas

The SVD structure of the inversion formulas can be easily appreciated by inserting the spectral expansion for $M^{-1}(\mathbf{q})$, given by

$$M_{mn}^{-1}(\mathbf{q}) = \sum_l \frac{1}{\sigma_{\mathbf{q}l}^2}[c_l(\mathbf{q})]_m[c_l^*(\mathbf{q})]_n, \quad (58)$$

into Eqs. (49) and (50). Here $c_l(\mathbf{q})$ is an eigenvector of $M(\mathbf{q})$ with eigenvalue $\sigma_{\mathbf{q}l}^2$:

$$\sum_n M_{mn}(\mathbf{q})[c_l(\mathbf{q})]_n = \sigma_{\mathbf{q}l}^2[c_l(\mathbf{q})]_m. \quad (59)$$

Then Eqs. (49) and (50) can be rewritten as

$$\begin{pmatrix}\delta\alpha(\mathbf{r})\\ \delta D(\mathbf{r})\end{pmatrix} = \sum_\mu \frac{1}{\sigma_\mu}f_\mu(\mathbf{r})\langle g_\mu,\, \phi\rangle. \quad (60)$$

Here $\mu = (\mathbf{q}, l)$ is a composite index, the symbol $\Sigma_\mu = \Sigma_l\int \mathrm{d}^2 q$, and σ_μ are the singular values and f_μ and g_μ the singular functions of the integral equation (37). Note that $\langle f_\mu, f_{\mu'}\rangle = \delta(\mu - \mu')$ and $\langle g_\mu, g_{\mu'}\rangle = \delta(\mu - \mu')$. The singular functions are given by the following expressions:

$$f_{\mathbf{q}l}(\mathbf{r}) = \frac{\exp(-i\mathbf{q}\cdot\boldsymbol{\rho})}{(2\pi)^2\sigma_{\mathbf{q}l}}\sum_n [c_l(\mathbf{q})]_n \times \begin{pmatrix} \kappa_A^*(\mathbf{q}/2 + \mathbf{p}_n, \mathbf{q}/2 - \mathbf{p}_n; z) \\ \kappa_D^*(\mathbf{q}/2 + \mathbf{p}_n, \mathbf{q}/2 - \mathbf{p}_n; z) \end{pmatrix}, \quad (61)$$

$$g_{\mathbf{q}l}(\mathbf{q}_1, \mathbf{q}_2) = \sum_n [c_l(\mathbf{q})]_n \delta(\mathbf{q}_1 - \mathbf{q}/2 - \mathbf{p}_n) \times \delta(\mathbf{q}_2 - \mathbf{q}/2 + \mathbf{p}_n). \quad (62)$$

Note that from the orthogonality condition of the singular functions, provided that $\sigma_\mu > 0$, it can be seen that there must exist a one-dimensional null space in which $\sigma_\mu = 0$. The SVD pseudoinverse solution belongs to the orthogonal complement of the null space.

D. Simultaneous versus Separate Reconstruction of $\delta\alpha$ and δD

It has been pointed out in Papers I and II that simultaneous reconstruction of $\delta\alpha$ and δD using scattering data obtained at a single modulation frequency is underdetermined. To perform simultaneous reconstruction of $\delta\alpha$ and δD, one needs at least two distinct modulation frequencies. Incorporation of multiple modulation frequencies can be achieved by noting that the functions κ_A and κ_D implicitly depend on ω through Eq. (7). Thus the functions κ_A and κ_D can be assigned an additional index (say, k) that labels the modulation frequency. In this case M can be viewed as a block matrix: The pair (k, k') will label a block corresponding to $\omega_k, \omega_{k'}$.

4. CYLINDRICAL GEOMETRY

We now turn our attention to the cylindrical geometry. In cylindrical coordinates (z, ρ, φ) the measurement surface is specified by $\rho = R$, where R is a constant, and the medium is confined to the region $\rho < R$.

The unperturbed Green's function in cylindrical coordinates can be found, for example, in Refs. 3 and 5. It can be represented as

$$G_0(\mathbf{r}, \mathbf{r}') = \frac{1}{2\pi}\sum_{m=-\infty}^{\infty}\int\frac{dq}{2\pi}\exp[im(\varphi - \varphi') + iq(z - z')]g(m, q; \rho, \rho'), \quad (63)$$

where $g(m, q; \rho, \rho')$ is given by a combination of modified Bessel and Hankel functions of the first kind, $I_m(x)$ and $K_m(x)$, respectively:

$$g(m, q; \rho, \rho') = \frac{1}{D_0}K_m(Q\rho_>)I_m(Q\rho_<) \quad \text{(free boundaries)}, \quad (64)$$

$$g(m, q; \rho, \rho') = \frac{1}{D_0}\left[K_m(Q\rho_>)I_m(Q\rho_<) - \frac{K_m(QR) + QlK_m'(QR)}{I_m(QR) + QlI_m'(QR)} \times I_m(Q\rho)I_m(Q\rho')\right] \quad \text{(boundary conditions)}, \quad (65)$$

where the prime denotes differentiation, $\rho_>$ and $\rho_<$ are the greater and the lesser of ρ and ρ', and $Q = Q(q)$ is given by Eq. (30), where q is now a scalar. When one of the arguments ρ or ρ' is on the measurement surface, Eqs. (64) and (65) become

$$g(m, q; \rho, R) = g(m, q; R, \rho) = \tilde{g}(m, q; \rho), \quad (66)$$

$$\tilde{g}(m, q; \rho) = \frac{1}{D_0}K_m(QR)I_m(Q\rho) \quad \text{(free boundaries)}, \quad (67)$$

$$\tilde{g}(m, q; \rho) = \frac{l}{D_0 R}\frac{I_m(Q\rho)}{I_m(QR) + QlI_m'(QR)} \quad \text{(boundary conditions)}. \quad (68)$$

The location of the sources and the detectors on the cylindrical measurement surface is characterized by the pairs of coordinates z_1, φ_1 and z_2, φ_2. The data function $\phi(z_1, \varphi_1; z_2, \varphi_2)$ satisfies the integral equation (3), which, with the use of Eqs. (63) and (66), can be written as

$$\phi(z_1, \varphi_1; z_2, \varphi_2) = \frac{\beta}{(2\pi)^4}\sum_{m_1, m_2=-\infty}^{\infty} \times \int dq_1 dq_2 \int_{\rho<R}\rho d\rho d\varphi dz \tilde{g}(m_1, q_1; \rho) \times \exp[im_1(\varphi - \varphi_1) + iq_1(z - z_1)] \times V\tilde{g}(m_2, q_2; \rho)\exp[im_2(\varphi_2 - \varphi) + iq_2(z_2 - z)]. \quad (69)$$

As in the planar case, we Fourier-transform the data function with respect to the variables $z_1, \varphi_1, z_2, \varphi_2$ according to

$$\phi(m_1, q_1; m_2, q_2) = \int_{-\infty}^{\infty}dz_1 dz_2 \int_0^{2\pi} d\varphi_1 d\varphi_2 \phi(\varphi_1, z_1; \varphi_2, z_2) \times \exp\{i[q_1 z_1 + q_2 z_2 + m_1\varphi_1 + m_2\varphi_2]\}. \quad (70)$$

The transformation (70) can be easily evaluated and yields

$$\phi(m_1, q_1; m_2, q_2) = \beta\int\rho d\rho d\varphi dz \exp[i(m_1\varphi + q_1 z)]\tilde{g}(m_1, q_1; \rho)V \times \exp[i(m_2\varphi + q_2 z)]\tilde{g}(m_2, q_2; \rho), \quad (71)$$

where we have used $\tilde{g}(-m, -q; \rho) = \tilde{g}(m, q; \rho)$.

Now we evaluate the action of the operator V, which leads to

$$\phi(m_1, q_1; m_2, q_2) = \int_0^R \rho d\rho \int_0^{2\pi} d\varphi \int_{-\infty}^{\infty} dz \times [\kappa_A(m_1, q_1, m_2, q_2; \rho)\delta\alpha(\rho, \varphi, z) + \kappa_D(m_1, q_1, m_2, q_2; \rho)\delta D(\rho, \varphi, z)] \times \exp[i(m_1 + m_2)\varphi + i(q_1 + q_2)z], \quad (72)$$

where

$$\kappa_A(m_1, q_1, m_2, q_2; \rho) = \beta\tilde{g}(m_1, q_1; \rho)\tilde{g}(m_2, q_2; \rho), \quad (73)$$

$$\kappa_D(m_1, q_1, m_2, q_2; \rho) = \beta\left[\frac{\partial\tilde{g}(m_1, q_1; \rho)}{\partial\rho}\frac{\partial\tilde{g}(m_2, q_2; \rho)}{\partial\rho} - \left(q_1 q_2 + \frac{m_1 m_2}{\rho^2}\right)\tilde{g}(m_1, q_1; \rho)\tilde{g}(m_2, q_2; \rho)\right]. \quad (74)$$

Equation (72) can be easily brought to the form of the one-dimensional integral equation that was inverted in Section 2. To this end we introduce new variables n, m, q, p_l according to $m_1 = m - n$, $m_2 = n$, $q_1 = q - p_l$, $q_2 = p_l$, where $q_l (l = 1,...,N_1)$ is a finite set of discrete wave numbers and n is an integer from a finite set containing N_2 numbers, and obtain

$$\phi(m - n, q - p_l; n, p_k) = \int_0^R [\kappa_A(m - n, q - p_l, n, p_l; \rho)a(\rho, m, q) + \kappa_D(m - n, q - p_l, n, p_l; \rho)b(\rho, m, q)]\rho d\rho, \quad (75)$$

where

$$a(\rho, m, q) = \int_0^{2\pi} d\varphi \int_{-\infty}^{\infty} dz\, \delta\alpha(\rho, \varphi, z)\exp[i(m\varphi + qz)], \quad (76)$$

$$b(\rho, m, q) = \int_0^{2\pi} d\varphi \int_{-\infty}^{\infty} dz\, \delta D(\rho, \varphi, z) \times \exp[i(m\varphi + qz)]. \quad (77)$$

For fixed m and q, Eq. (75) can be inverted as discussed in Section 2. The functions $\delta\alpha(\mathbf{r})$ and $\delta D(\mathbf{r})$ are then obtained by inverting the Fourier transforms (76) and (77). The final result has the form

$$\delta\alpha(\rho, \varphi, z) = \frac{1}{(2\pi)^2\rho}\sum_{m=-\infty}^{\infty}\exp(-im\varphi)\int_{-\infty}^{\infty} dq \exp(-iqz) \times \sum_{nl,n'l'}\kappa_A^*(m - n, q - p_l, n, p_l; \rho)M^{-1}_{nl,n'l'}(m, q) \times \phi(m - n', q - p_{l'}; n', p_{l'}), \quad (78)$$

$$\delta D(\rho, \varphi, z) = \frac{1}{(2\pi)^2\rho}\sum_{m=-\infty}^{\infty}\exp(-im\varphi)\int_{-\infty}^{\infty} dq \exp(-iqz) \times \sum_{nl,n'l'}\kappa_D^*(m - n, q - p_l, n, p_l; \rho)M^{-1}_{nl,n'l'}(m, q) \times \phi(m - n', q - p_{l'}; n', p_{l'}), \quad (79)$$

$$M_{nl,n'l'}(m, q) = \int_0^R [\kappa_A(m - n, q - p_l, n, p_l; \rho) \times \kappa_A^*(m - n', q - p_{l'}, n', p_{l'}; \rho) + \kappa_D(m - n, q - p_l, n, p_l; \rho) \times \kappa_D^*(m - n', q - p_{l'}, n', p_{l'}; \rho)]d\rho. \quad (80)$$

A few comments on the above inversion formulas need to be made. First, the rows and the columns of the matrix M are labeled by two indices, n and l. Therefore M can be considered a block matrix. The total number of elements in M is $(N_1N_2)^2$. Note that the rows and the columns of M can also be characterized by two indices in the case of the planar measurement surface, since the discrete vectors $\mathbf{q}_m$ are two dimensional in this case and can be represented as $\mathbf{q}_m = \hat{\mathbf{e}}_x q_{m_x} + \hat{\mathbf{e}}_y q_{m_y}$. Second, the expression for $M_{nl,n'l'}(m, q)$ [Eq. (80)] involves integrals containing products of four Bessel functions or their first derivatives. These integrals must be computed numerically.

5. SPHERICAL GEOMETRY

In the spherical geometry with $\mathbf{r} = (r, \theta, \varphi)$, the data function is measured on the surface $r = R$ and the medium is located inside the sphere. The unperturbed Green's function can be represented as[3,5]

$$G_0(\mathbf{r}, \mathbf{r}') = \sum_{l=0}^{\infty}\sum_{m=-l}^{l} g(l; r, r')Y_{lm}(\hat{\mathbf{r}})Y_{lm}^*(\hat{\mathbf{r}}'), \quad (81)$$

where the $Y_{lm}(\hat{\mathbf{r}})$ are spherical harmonics and $\hat{\mathbf{r}} = \mathbf{r}/r$ is a unit vector characterized by the angular variables θ and φ. The radial function $g(l; r, r')$ is given by a linear combination of modified spherical Bessel and Hankel functions of the first kind, $i_l(x)$ and $k_l(x)$, respectively:

$$g(l; r, r') = \frac{2k}{\pi D_0}i_l(kr_<)k_l(kr_>) \quad \text{(free boundaries)}, \quad (82)$$

$$g(l; r, r') = \frac{2k}{\pi D_0}\left[i_l(kr_<)k_l(kr_>) - \frac{k_l(kR) + klk_l'(kR)}{i_l(kR) + kli_l'(kR)}i_l(kr)i_l(kr')\right] \quad \text{(boundary conditions)}, \quad (83)$$

where $r_>$ and $r_<$ are the greater and the lesser of r and r'. As in the cases of the planar and cylindrical geometries, we simplify the above expression by observing that either r or r' must be equal to R in the expression for the data function:

$$g(l;\, r,\, R) = g(l;\, R,\, r) = \tilde{g}(l;\, r), \tag{84}$$

$$\tilde{g}(l;\, r) = \frac{2k^2}{\pi D_0} k_l(kR) i_l(kr) \qquad \text{(free boundaries)}, \tag{85}$$

$$\tilde{g}(l;\, r) = \frac{l}{D_0 R^2} \frac{i_l(kr)}{i_l(kR) + kli_l'(kR)} \qquad \text{(boundary conditions)}. \tag{86}$$

The data function defined on the spherical surface is a function of the angular variables θ_1, φ_1 and θ_2, φ_2 of the sources and the detectors, respectively. For simplicity, we will use the unit vectors $\hat{\mathbf{r}}_1 = (\theta_1,\, \varphi_1)$ and $\hat{\mathbf{r}}_2 = (\theta_2,\, \varphi_2)$. Then the data function can be written as

$$\phi(\hat{\mathbf{r}}_1,\, \hat{\mathbf{r}}_2) = \beta \sum_{l_1,l_2} \sum_{m_1,m_2} \int \mathrm{d}^3 r \tilde{g}(l_1;\, r) Y_{l_1 m_1}(\hat{\mathbf{r}}_1) \times Y^*_{l_1 m_1}(\hat{\mathbf{r}}) V \tilde{g}(l_2;\, r) Y_{l_2 m_2}(\hat{\mathbf{r}}) Y^*_{l_2 m_2}(\hat{\mathbf{r}}_2). \tag{87}$$

Instead of Fourier-transforming the data function as in the planar and cylindrical geometries, we project it onto spherical harmonics and define

$$\phi(l_1,\, m_1;\, l_2,\, m_2) = \int \phi(\hat{\mathbf{r}}_1,\, \hat{\mathbf{r}}_2) Y^*_{l_1 m_1}(\hat{\mathbf{r}}_1) Y_{l_2 m_2}(\hat{\mathbf{r}}_2) \mathrm{d}^2\hat{\mathbf{r}}_1 \mathrm{d}^2\hat{\mathbf{r}}_2. \tag{88}$$

The equation for the projected data function becomes

$$\phi(l_1,\, m_1;\, l_2,\, m_2) = \beta \int \mathrm{d}^3 r \tilde{g}(l_1;\, r) Y^*_{l_1 m_1}(\hat{\mathbf{r}}) V \tilde{g}(l_2;\, r) Y_{l_2 m_2}(\hat{\mathbf{r}}). \tag{89}$$

Next, we need to evaluate the action of the operator $V = \delta\alpha - \nabla_{\mathbf{r}} \cdot \delta D \nabla_{\mathbf{r}}$ and bring the integral equation (89) to one-dimensional form. This task faces two difficulties. First, the term proportional to $\delta\alpha$ can be trivially calculated, but it contains the product of two spherical functions, $Y^*_{l_1 m_1}(\hat{\mathbf{r}}) Y_{l_2 m_2}(\hat{\mathbf{r}})$, in the integrand. In the planar and cylindrical geometries, we encountered a product of two exponentials that was trivially expressed as a single exponential. However, the product of two spherical functions is expressible not as a *single* spherical function but rather by a linear combination of spherical functions with different indices. The problem is mathematically similar to the addition of two quantized angular momenta. Second, evaluation of the term proportional to δD is quite involved. Although, in principle, we can express the operator $\nabla_{\mathbf{r}} \cdot \delta D \nabla_{\mathbf{r}}$ in terms of raising and lowering operators, L_+ and L_-, this approach will lead to the appearance of spherical functions with magnetic numbers shifted by 0, ± 1. Instead, we first express the operator in question in terms of L^2, where $\mathbf{L} = -i\mathbf{r} \times \nabla$ is the angular momentum operator, and then expand the product $Y^*_{l_1 m_1} Y_{l_2 m_2}$ as a linear combination of Y_{lm} and note that Y_{lm} is an eigenfunction of L^2.

As shown in Appendix A, the term proportional to δD in Eq. (89) can be written as

$$\int \mathrm{d}^3 r \tilde{g}(l_1;\, r) Y^*_{l_1 m_1}(\hat{\mathbf{r}}) (-\nabla \cdot \delta D \nabla) \tilde{g}(l_2;\, r) Y_{l_2 m_2}(\hat{\mathbf{r}}) = \int \mathrm{d}^3 r \delta D \left[\frac{\partial \tilde{g}(l_1;\, r)}{\partial r} \frac{\partial \tilde{g}(l_2;\, r)}{\partial r} - \frac{\tilde{g}(l_1;\, r) \tilde{g}(l_2;\, r)}{r^2} \times \frac{L^2 - l_1(l_1+1) - l_2(l_2+1)}{2} \right] Y^*_{l_1 m_1} Y_{l_2 m_2}. \tag{90}$$

Next, we expand $Y^*_{l_1 m_1} Y_{l_2 m_2}$ as

$$Y^*_{l_1 m_1} Y_{l_2 m_2} = \sum_{lm} C^{l_1 m_1 l_2 m_2}_{lm} Y^*_{lm}, \tag{91}$$

where $C^{l_1 m_1 l_2 m_2}_{lm}$ is, up to a multiplicative constant, the Clebsch–Gordan coefficient, which defines the transformation matrix from the full orthonormal set of $(2l_1 + 1)(2l_2 + 1)$ states $|l_1 m_1 l_2 m_2\rangle$ to an orthonormal set $|lm\rangle$ (for fixed l_1 and l_2). Now we can rewrite Eq. (89) as follows:

$$\phi(l_1,\, m_1;\, l_2,\, m_2) = \beta \sum_{lm} C^{l_1 m_1 l_2 m_2}_{lm} \int \mathrm{d}^3 r \left\{ \tilde{g}(l_1;\, r) \tilde{g}(l_2;\, r) \delta\alpha(\mathbf{r}) + \delta D(\mathbf{r}) \left[\frac{\partial \tilde{g}(l_1;\, r)}{\partial r} \frac{\partial \tilde{g}(l_2;\, r)}{\partial r} - \frac{\tilde{g}(l_1;\, r) \tilde{g}(l_2;\, r)}{r^2} \times \frac{l(l+1) - l_1(l_1+1) - l_2(l_2+1)}{2} \right] \right\} Y^*_{lm}(\hat{\mathbf{r}}). \tag{92}$$

The coefficients $C^{l_1 m_1 l_2 m_2}_{lm} = \int Y^*_{l_1 m_1} Y_{lm} Y_{l_2 m_2} \mathrm{d}\Omega$ are expressed in terms of $3j$-symbols as

$$C^{l_1 m_1 l_2 m_2}_{lm} = (-1)^{m+m_2} \left[\frac{(2l_1+1)(2l+1)(2l_2+1)}{4\pi} \right]^{1/2} \times \begin{pmatrix} l_1 & l & l_2 \\ 0 & 0 & 0 \end{pmatrix} \begin{pmatrix} l_1 & l & l_2 \\ -m_1 & m & m_2 \end{pmatrix}. \tag{93}$$

Now we use the following symmetry and orthogonality properties of the $3j$-symbols:

$$\begin{pmatrix} l_1 & l & l_2 \\ -m_1 & m & m_2 \end{pmatrix} = \begin{pmatrix} l_1 & l_2 & l \\ m_1 & -m_2 & -m \end{pmatrix}, \tag{94}$$

$$\sum_{m_1=-l_1}^{l_1} \sum_{m_2=-l_2}^{l_2} \begin{pmatrix} l_1 & l_2 & l \\ m_1 & m_2 & -m \end{pmatrix} \begin{pmatrix} l_1 & l_2 & l' \\ m_1 & m_2 & -m' \end{pmatrix} = \frac{\delta_{ll'} \delta_{mm'}}{2l+1}; \tag{95}$$

and we define a transformed data function $\psi(l,\, m;\, l_1,\, l_2)$ according to

$$\psi(l,\, m;\, l_1,\, l_2) = \left[\frac{4\pi(2l+1)}{(2l_1+1)(2l_2+1)}\right]^{1/2} \times \begin{pmatrix} l_1 & l & l_2 \\ 0 & 0 & 0 \end{pmatrix}^{-1} \sum_{m_1=-l_1}^{l_1} \sum_{m_2=-l_2}^{l_2} (-1)^{m_2-m} \times \begin{pmatrix} l_1 & l_2 & l \\ m_1 & m_2 & -m \end{pmatrix} \phi(l_1,\, m_1;\, l_2,\, -m_2). \quad (96)$$

Then it is easy to see that

$$\psi(l,\, m;\, l_1,\, l_2) = \int_0^R r^2 \mathrm{d}r \int \mathrm{d}\Omega [\kappa_A(l_1,\, l_2;\, r)\delta\alpha(\mathbf{r}) + \kappa_D(l,\, l_1,\, l_2;\, r)\delta D(\mathbf{r})] Y^*_{lm}(\hat{\mathbf{r}}), \quad (97)$$

where

$$\kappa_A(l_1,\, l_2;\, r) = \beta \tilde{g}(l_1;\, r)\tilde{g}(l_2;\, r), \quad (98)$$

$$\kappa_D(l,\, l_1,\, l_2;\, r) = \beta\left[\frac{\partial\tilde{g}(l_1;\, r)}{\partial r}\frac{\partial\tilde{g}(l_2;\, r)}{\partial r} - \frac{\tilde{g}(l_1;\, r)\tilde{g}(l_2;\, r)}{r^2} \times \frac{l(l+1) - l_1(l_1+1) - l_2(l_2+1)}{2}\right]. \quad (99)$$

Equation (97) is inverted as follows. Define

$$a(l,\, m;\, r) = \int \delta\alpha(\mathbf{r}) Y^*_{lm}(\hat{\mathbf{r}})\mathrm{d}\Omega, \quad (100)$$

$$b(l,\, m;\, r) = \int \delta D(\mathbf{r}) Y^*_{lm}(\hat{\mathbf{r}})\mathrm{d}\Omega, \quad (101)$$

which satisfy the one-dimensional integral equation

$$\psi(l,\, m;\, l_1,\, l_2) = \int_0^R r^2 \mathrm{d}r [\kappa_A(l_1,\, l_2;\, r)a(l,\, m;\, r) + \kappa_D(l,\, l_1,\, l_2;\, r)b(l,\, m;\, r)], \quad (102)$$

which is inverted for a fixed pair $(l,\, m)$ as described in Section 2:

$$a(l,\, m;\, r) = \frac{1}{r^2} \sum_{l_1,l_2,l_1',l_2'} \kappa^*_A(l_1,\, l_2;\, r) \times M^{-1}_{l_1l_2,l_1'l_2'}(l)\psi(l,\, m;\, l_1',\, l_2'), \quad (103)$$

$$b(l,\, m;\, r) = \frac{1}{r^2} \sum_{l_1,l_2,l_1',l_2'} \kappa^*_D(l_1,\, l_2;\, r) \times M^{-1}_{l_1l_2,l_1'l_2'}(l)\psi(l,\, m;\, l_1',\, l_2'), \quad (104)$$

$$M^{-1}_{l_1l_2,l_1'l_2'}(l) = \int_0^r [\kappa_A(l_1,\, l_2;\, r)\kappa^*_A(l_1',\, l_2';\, r) + \kappa_D(l,\, l_1,\, l_2;\, r)\kappa^*_D(l,\, l_1',\, l_2';\, r)]\mathrm{d}r. \quad (105)$$

The functions $\delta\alpha$ and δD are obtained by substitution of Eqs. (103) and (104) into Eqs. (100) and (101), respectively, and by using the orthogonality of the spherical functions, we obtain the inversion formulas:

$$\delta\alpha(\mathbf{r}) = \sum_{lm} a(l,\, m;\, r)Y_{lm}(\hat{\mathbf{r}}) = \sum_{lm} Y_{lm}(\hat{\mathbf{r}}) \sum_{l_1,l_2,l_1',l_2' \in \sigma(l)} \frac{\kappa^*_A(l_1,\, l_2;\, r)}{r^2} \times M^{-1}_{l_1l_2,l_1'l_2'}(l)\psi(l,\, m;\, l_1',\, l_2'), \quad (106)$$

$$\delta D(\mathbf{r}) = \sum_{lm} b(l,\, m;\, r)Y_{lm}(\hat{\mathbf{r}}) = \sum_{lm} Y_{lm}(\hat{\mathbf{r}}) \sum_{l_1,l_2,l_1',l_2' \in \sigma(l)} \frac{\kappa^*_D(l,\, l_1,\, l_2;\, r)}{r^2} \times M^{-1}_{l_1l_2,l_1'l_2'}(l)\psi(l,\, m;\, l_1',\, l_2'). \quad (107)$$

In the above formulas $\sigma(l)$ denotes the set of allowable values of l_1, l_2 (which depends on l). Indeed, the transformed data function $\psi(l,\, m;\, l_1,\, l_2)$ is defined not for all possible values of its arguments but only when the $3j$-symbol

$$\begin{pmatrix} l_1 & l & l_2 \\ 0 & 0 & 0 \end{pmatrix}$$

is not zero; in the opposite case the function $\psi(l,\, m;\, l_1,\, l_2)$ must be set identically to zero. The conditions for the above $3j$-symbol to be nonzero are that $|l_1 - l_2| \leq l \leq l_1 + l_2$ (which is the usual condition for addition of two angular momenta) and also that the sum $l_1 + l_2 + l$ be an even number (which follows from the symmetry of $3j$-symbols under the reflection of the z axis). The values of l_1 and l_2 that satisfy these two conditions for a given l are illustrated in Fig. 1.

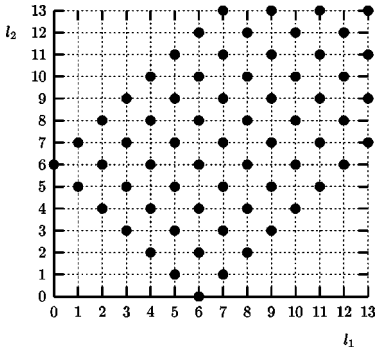

Fig. 1. Set $\sigma(l)$ of allowable values of l_1 and l_2 for $l = 6$. Note that $\sigma(l)$ is infinite, and the plot must be continued to infinitely large numbers of l_1 and l_2 lying on or between the lines $l_2 = l_1 \pm l$ and $l_2 = l - l_1$ as shown.

Next, we simplify expression (96) for the transformed data function ψ. First, we note that the terms in summation (96) vanish unless $m_1 + m_2 - m = 0$. This allows us to perform one of the summations, and we arrive at the following expression:

$$\psi(l, m; l_1, l_2) = \left[\frac{4\pi(2l+1)}{(2l_1+1)(2l_2+1)}\right]^{1/2} \begin{pmatrix} l_1 & l & l_2 \\ 0 & 0 & 0 \end{pmatrix}^{-1} \times \sum_{m_1=\max(-l_1,\, m-l_2)}^{\min(l_1,\, m+l_2)} (-1)^{m_1} \begin{pmatrix} l_1 & l_2 & l \\ m_1 & m-m_1 & -m \end{pmatrix} \times \phi(l_1, m_1; l_2, m_1 - m), \tag{108}$$

where we also took into account the fact that the $3j$-symbol

$$\begin{pmatrix} l_1 & l_2 & l \\ m_1 & m-m_1 & -m \end{pmatrix}$$

vanishes unless $-l_1 \leqslant m_1 \leqslant l_1$ and $-l_2 \leqslant m - m_1 \leqslant l_2$. It is easy to verify that for a given l and an allowable pair l_1, l_2 from the set $\sigma(l)$ (illustrated in Fig. 1), the summation in Eq. (108) has at least one nonvanishing term.

Note that the matrix $M(l)$ depends on l not only because of the explicit dependence of κ_D on l but also because the set of allowable values of l_1, l_2 itself depends on l. If we assume *a priori* that $\delta D = 0$, the definition of M does not contain κ_D [the second term in Eq. (105) must be omitted in this case]. Although κ_A does not depend on l explicitly, the operator M still depends on this parameter through the dependence $\sigma(l)$. However, in the general case, M does not depend on the magnetic quantum number m. Since the only two quantities in Eqs. (106) and (107) that depend on m are Y_{lm} and ψ, the summation over this index (from $-l$ to l) should be carried out first.

6. DEPTH RESOLUTION

The inversion formulas derived in this paper take advantage of certain geometrical symmetries. The variables on which the inversion formulas depend are effectively separated into "transverse" and "longitudinal" types. Thus, in the case of the planar geometry, the transverse variable is $\boldsymbol{\rho} = (x, y)$. For the cylindrical geometry the transverse variables are z and φ, and for the spherical geometry they are θ and φ. We saw that the singular functions are naturally expressed in terms of orthonormal functions of the transverse variables (exponentials for the planar and cylindrical geometries and spherical functions for the spherical geometry). The orthogonality in the longitudinal variables is, however, achieved by taking a linear superposition of nonorthogonal functions κ_A and κ_D. The coefficients in this superposition are obtained by inverting the overlap matrix M, which, in general, has an extremely small determinant. This fact sets a limit on the depth resolution, whose origin is due purely to numerical precision. In Refs. 6 and 7, we have studied this resolution limit in the planar geometry with various types of boundary conditions and source–detector arrangements. In particular, it was found that the depth resolution is best in the two-plane detection scheme when the sources and the detectors are located on different planes.

The mathematical problem of depth resolution is best revealed by considering the inversion formulas for forward data generated by $\delta\alpha$ and δD that are homogeneous in the transverse variables. Thus, in the planar geometry, we set

$$\delta\alpha(\mathbf{r}) = a_A \delta(z - z_A), \qquad \delta D(\mathbf{r}) = a_D \delta(z - z_D), \tag{109}$$

where $0 < z_A, z_D < L$. We intend to recover the one-dimensional functions $\delta\alpha(z)$ and $\delta D(z)$ by using the forward data generated by Eqs. (109):

$$\phi(\mathbf{q}_1, \mathbf{q}_2) = (2\pi)^2 \delta(\mathbf{q}_1 + \mathbf{q}_2)[a_A \kappa_A(\mathbf{q}_1, \mathbf{q}_2; z_A) + a_D \kappa_D(\mathbf{q}_1, \mathbf{q}_2; z_D)]. \tag{110}$$

Substituting this expression into the inversion formulas (49) and (50), we obtain

$$\begin{pmatrix} \delta\alpha \\ \delta D \end{pmatrix} = \sum_{m,n} \begin{pmatrix} \kappa_A^*(\mathbf{p}_m, -\mathbf{p}_m; z) \\ \kappa_D^*(\mathbf{p}_m, -\mathbf{p}_m; z) \end{pmatrix} \times M_{mn}^{-1}(0)[a_A \kappa_A(\mathbf{p}_n, -\mathbf{p}_n; z_A) + a_D \kappa_D(\mathbf{p}_n, -\mathbf{p}_n; z_D)]. \tag{111}$$

For simplicity, we consider the case $a_D = 0$ and set *a priori* $\delta D = 0$. Then the inversion formula becomes

$$\delta\alpha = a_A \sum_{mn} \kappa_A^*(\mathbf{p}_m, -\mathbf{p}_m; z) M_{mn}^{-1} \kappa_A(\mathbf{p}_n, -\mathbf{p}_n; z_A), \tag{112}$$

$$M_{mn} = \int_0^L \kappa_A(\mathbf{p}_m, -\mathbf{p}_m; z) \kappa_A^*(\mathbf{p}_n, -\mathbf{p}_n; z) \mathrm{d}z. \tag{113}$$

Now we expand $\kappa(\mathbf{p}_m, -\mathbf{p}_m; z)$ as

$$\kappa(\mathbf{p}_m, -\mathbf{p}_m; z) = \sum_n A_{mn} \varphi_n(z), \tag{114}$$

where $\varphi_n(z)$ is a complete orthonormal set and A is a matrix of coefficients. Evidently, $M = AA^*$, and thus Eq. (112) may be rewritten as

$$\delta\alpha = a_A \sum_{m,n} \varphi_n^*(z) \varphi_m(z_A) [A^*(AA^*)^{-1} A]_{mn}. \tag{115}$$

If A^{-1} exists, then $[A^*(AA^*)^{-1}A]_{mn} = \delta_{mn}$ and the expression on the right-hand side of Eq. (115) becomes a delta function. However, the matrix A is not invertible for any finite number of vectors $\mathbf{p}_m$, since it is not square. Only when $\mathbf{p}_m$ becomes continuous can A^{-1} be formally defined. In Refs. 3 and 5, we have shown that A^{-1} exists in all three geometries (in the continuous limit) by reducing the relevant integral equation to the Fourier–Laplace form. Numerically, it is expected that as the number of discrete vectors $\mathbf{p}_m$ increases, the function on the right-hand side of Eq. (115) acquires an increasingly narrow peak centered near $z = z_A$. The minimum width of this peak is, however, limited by numerical precision rather than by the number of $\mathbf{p}_m$'s.

Note that a similar analysis of depth resolution with respect to the variables ρ and r can be applied to the cylindrical and spherical geometries, respectively.

To illustrate the nature of the depth resolution, we present the results of numerical reconstruction of $\delta\alpha$ with the forward data generated for an infinite planar absorber (109) and also for a point absorber of the form

$$\delta\alpha = a_A \delta(z - z_A)\delta(\mathbf{p}). \tag{116}$$

In the latter case the reconstruction is carried out along the line $\boldsymbol{\rho}=0$, which connects the absorber and the two measurement planes. We used the biplanar geometry with $L = \lambda_{\text{diff}} \equiv 2\pi k^{-1}$ and $\omega=0$. Forty discrete collinear vectors $\mathbf{p}_m = \hat{\mathbf{e}}_x \Delta p(m - 1)$ $(m = 1,..., N,\ N = 40)$ were used with $\Delta p = k^{-1}$. Note that even though the vectors $\mathbf{p}_m$ are restricted to a one-dimensional subspace, the inverse problem is well defined. It was found that further increasing the number N or placing the vectors $\mathbf{p}_m$ on a two-dimensional surface did not provide increased depth resolution. All curves were normalized to their maximum values. The regularization parameter was set to be $\epsilon = 10^{-18}$ in a double-precision code.

The results are shown in Figs. 2–4. Note that the case of free boundaries for an infinite planar absorber, with the sources and the detectors located on different planes, is degenerate, since, as can be easily seen from Eqs. (54) and (56), $\kappa_A(\mathbf{p}_m, -\mathbf{p}_m; z)$=constant and the depth resolution is completely lost. In all other cases the arrangement when the sources and the detectors are located on different planes provides better depth resolution; inclusion of additional data with the sources and the detectors on the same plane provides a very moderate increase in resolution.

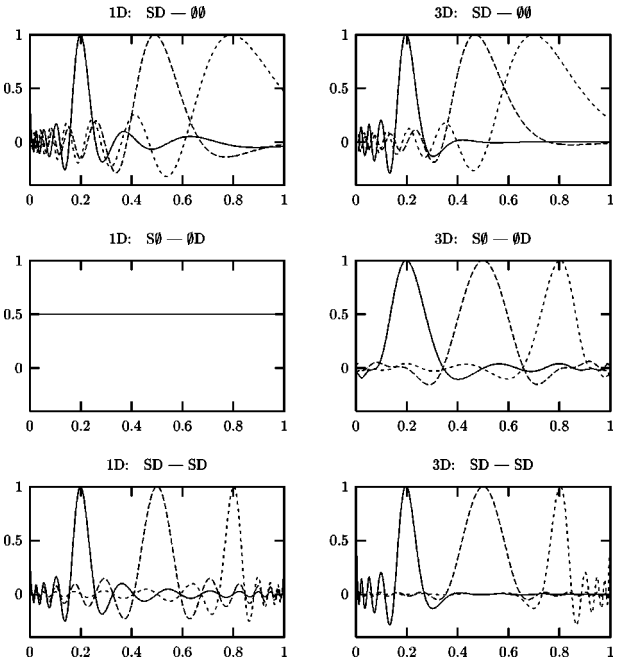

Fig. 2. Depth resolution for free boundary conditions. Left column: forward data simulated for the infinite plane absorber (109); right column: forward data generated for the point absorber (116); top row: sources and detectors on the same plane; middle row: sources and detectors on different planes; bottom row: simultaneous SVD solution for sources and detectors on plane $z = 0$, sources and detectors on plane $z = L$, and sources on plane $z = 0$ and detectors on plane $z = L$. Solid curves correspond to $z_A = 0.2L$, long-dashed curves correspond to $z_A = 0.5L$, and short-dashed curves correspond to $z_A = 0.8L$.

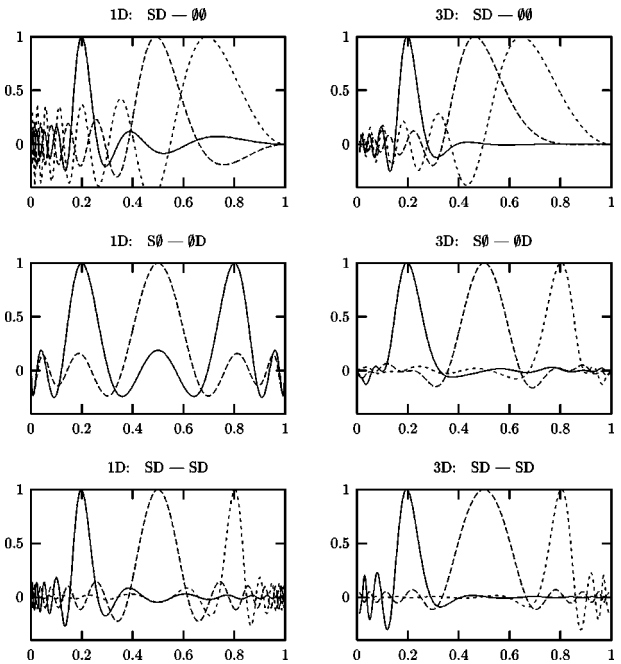

Fig. 3. Depth resolution for absorbing boundary conditions; parameters are the same as those in Fig. 2.

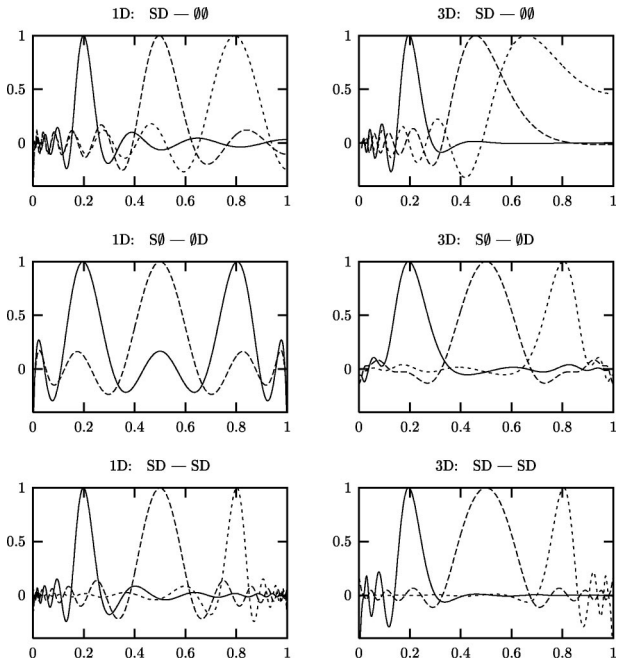

Fig. 4. Depth resolution for reflecting boundary conditions; parameters are the same as those in Fig. 2.

7. NUMERICAL RESULTS

We now illustrate the inversion formulas derived in this paper with numerical examples. Reconstructions with planar boundaries have been implemented in Refs. 6 and 7, and the depth resolution in this case is illustrated in Section 6. Here we will focus on the cylindrical geometry

including simultaneous reconstruction of the absorption and diffusion coefficients. Absorbing boundary conditions are used throughout this section.

We begin with the single-frequency case in which δD is known to be zero *a priori*. Continuous-wave imaging ($\omega=0$) is used. In Fig. 5 we show the reconstruction of $\delta\alpha$ for forward data generated by a point absorber located at the point $\rho = 0.5R$, $\varphi=\pi$, $z = 0$. The following parameters were used: The summation over m in Eq. (78) was from -10 to 10, and the integration over q was from $-16R^{-1}$ to $16R^{-1}$. Convergence was demonstrated by both increasing the limits of summation and integration and decreasing the step size in integration over q. It can be seen from Eq. (80) that the matrix M is labeled by two indices: n and k. The one-dimensional vectors p_k ($k = 1, 2,...$) are parallel to the cylinder axis and are discrete but otherwise arbitrary. In principle, a two-dimensional parameter space (k, n) can be used to construct M. However, we found that this does not lead to improved resolution compared with the case when one of the parameters is fixed. In Fig. 5 we have used $n = 0$ and $p_k = R^{-1}k$, where $k = 0, \pm1,..., \pm10$. The matrix elements of M were calculated numerically by using a sixth-order Simpson's rule. The diffuse wave number was set to $k = 2\pi/R$, so that $\lambda_{\text{diff}} \equiv 2\pi/k = R$. The tomographic slices in Fig. 5 are drawn perpendicular to the cylinder axis at different values of z. It can be seen from the figure that the maximum intensity is located in the correct location and that the resolution is significantly better than the limit set by the diffuse wavelength λ_{diff} or the cylinder radius R. The resolution changes when the absorber is placed at different depths ρ. This is illustrated in Fig. 6. As could be expected, the resolution is best when the absorber is close to the surface.

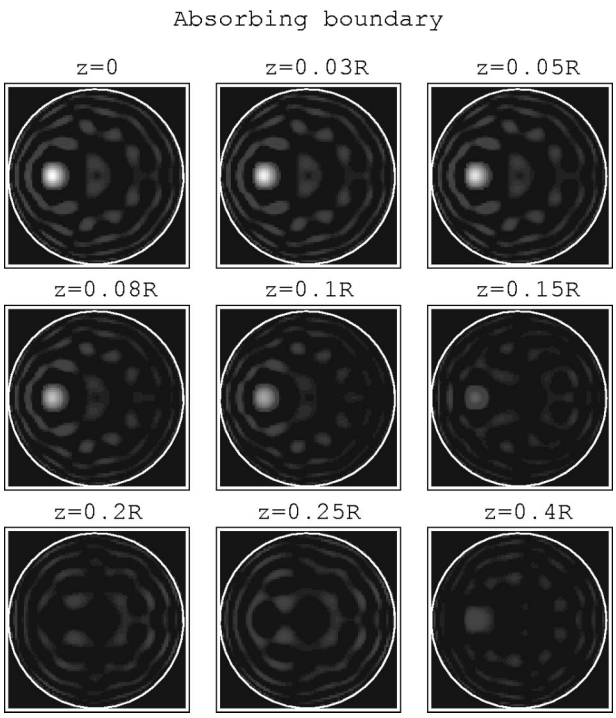

Fig. 5. Reconstruction of the absorption coefficient $\delta\alpha$ with the assumption $\delta D = 0$ according to Eq. (78) in the cylindrical geometry. A point absorber is placed at $\rho = 0.5R$, $\varphi = \pi$, $z = 0$. The slices shown are perpendicular to the cylinder axis and have different z coordinates as indicated in the figure (the $z = 0$ slice is drawn directly through the absorber). The same linear gray scale is employed in all the plots.

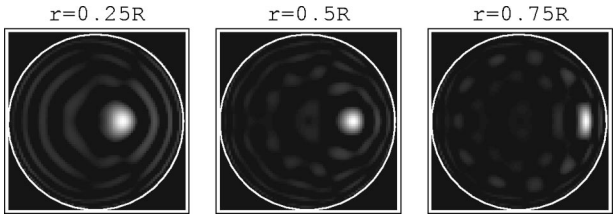

Fig. 6. Reconstruction of the absorption coefficient $\delta\alpha$ with the assumption $\delta D = 0$ according to Eq. (78) in the cylindrical geometry. The forward data are generated for a point absorber located at $\varphi = 0$, $z = 0$, and $\rho = 0.25R$, $0.5R$, $0.75R$ as indicated. Each reconstructed function is normalized to its maximum, and a linear gray scale is employed.

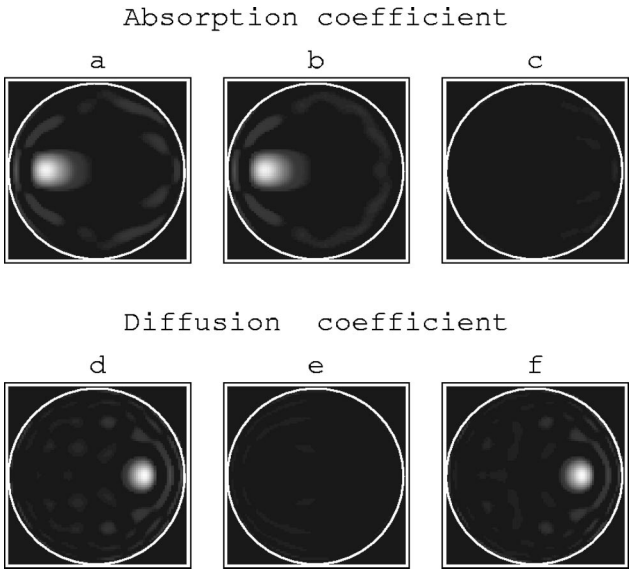

Fig. 7. Simultaneous reconstruction of $\delta\alpha$ and δD. In images a and d, the forward data are generated for a point absorber located at $\rho = 0.5R$, $\varphi = \pi$, $z = 0$ and a point diffusing inhomogeneity located at $\rho = 0.5R$, $\varphi = 0$, $z = 0$. In images b and e only the absorbing inhomogeneity, and in c and f only the diffusion inhomogeneity, were used to generate the forward data. Images a–c (and d–f) use the same linear gray scale.

Now we turn to the simultaneous reconstruction of $\delta\alpha$ and δD. We have chosen the first modulation frequency ω_1 to be zero, and the second was chosen from the condition $\omega_2 = \alpha_0$, so that $k_2^2 = (\alpha_0 - i\omega_2)/D_0 = k_1^2(1 - i)$, where $k_1^2 = \alpha_0/D_0$. For typical biological tissues $\alpha_0 \approx 1$ GHz. Therefore, if the above condition is satisfied, the oscillator frequency $\nu_2 = \omega_2/2\pi$ is of the order of 100 MHz.

In Fig. 7 we show the simultaneous reconstruction of $\delta\alpha$ and δD. The upper row of images contains reconstructions of $\delta\alpha$, and the bottom row contains reconstructions of δD. All tomographic slices are drawn in the $z = 0$ plane. In images a and d, the forward data were generated for a point absorber located at $\rho = 0.5R$, $\varphi = \pi$, $z = 0$ and a point diffusing inhomogeneity at $\rho = 0.5R$, $\varphi = 0$, $z = 0$. In images b and e only the absorbing inhomogeneity, and in c and f only the diffusion

inhomogeneity, were used to generate the forward data. As can be seen from the figure, both absorption and diffusion coefficients are reliably reconstructed with two modulation frequencies. It can be noted that the resolution is somewhat higher for the reconstruction of the diffusion coefficient. As is discussed in Ref. 6, this is explained by the fact that the diffusing inhomogeneity of the same "numerical" strength influences the data function more strongly than an absorbing inhomogeneity.

APPENDIX A: EVALUATION OF THE ACTION OF THE OPERATOR $\nabla \cdot \delta D \nabla$ IN THE SPHERICAL GEOMETRY

To evaluate

$$\int \mathrm{d}^3 r \tilde{g}(l_1; r) Y^*_{l_1 m_1}(\hat{\mathbf{r}})(-\nabla \cdot \delta D \nabla)\tilde{g}(l_2; r) Y_{l_2 m_2}(\hat{\mathbf{r}}), \tag{A1}$$

we act with the operator ∇ in expression (A1) to the left and simultaneously change the overall sign of the expression, since ∇ is anti-Hermitian. Thus we arrive at an expression of the form $[\nabla F(\mathbf{r})] \cdot [\nabla G(\mathbf{r})]$, where $F(\mathbf{r}) = \tilde{g}(l_1; r) Y^*_{l_1 m_1}(\hat{\mathbf{r}})$ and $G(\mathbf{r}) = \tilde{g}(l_2; r) Y_{l_2 m_2}(\hat{\mathbf{r}})$. We use the identity

$$\nabla F \cdot \nabla G = \frac{(\mathbf{r} \cdot \nabla F)(\mathbf{r} \cdot \nabla G) + (\mathbf{r} \times \nabla F) \cdot (\mathbf{r} \times \nabla G)}{r^2} \tag{A2}$$

and the following relations:

$$\begin{aligned} \mathbf{r} \times \nabla F &= i \tilde{g}(l_1; r) \mathbf{L} Y^*_{l_1 m_1}, \\ \mathbf{r} \times \nabla G &= i \tilde{g}(l_2; r) \mathbf{L} Y_{l_2 m_2}; \end{aligned} \tag{A3}$$

$$\begin{aligned} \mathbf{r} \cdot \nabla F &= r \frac{\partial \tilde{g}(l_1; r)}{\partial r} Y^*_{l_1 m_1}, \\ \mathbf{r} \cdot \nabla G &= r \frac{\partial \tilde{g}(l_2; r)}{\partial r} Y_{l_2 m_2}, \end{aligned} \tag{A4}$$

where $\mathbf{L} = -i \mathbf{r} \times \nabla$. Upon substitution of Eqs. (A3) and (A4) into Eq. (A2), we obtain

$$\begin{aligned} \nabla F \cdot \nabla G = {} & \frac{\partial \tilde{g}(l_1; r)}{\partial r} \frac{\partial \tilde{g}(l_2; r)}{\partial r} Y^*_{l_1 m_1} Y_{l_2 m_2} \\ & - \frac{\tilde{g}(l_1; r) \tilde{g}(l_2; r)}{r^2} \mathbf{L} Y^*_{l_1 m_1} \cdot \mathbf{L} Y_{l_2 m_2}. \end{aligned} \tag{A5}$$

Next, we act with operator L^2 on $Y^*_{l_1 m_1} Y_{l_2 m_2}$; i.e.,

$$\begin{aligned} L^2 Y^*_{l_1 m_1} Y_{l_2 m_2} = {} & 2 \mathbf{L} Y^*_{l_1 m_1} \cdot \mathbf{L} Y_{l_2 m_2} \\ & + Y^*_{l_1 m_1} L^2 Y_{l_2 m_2} + Y_{l_2 m_2} L^2 Y^*_{l_1 m_1}, \end{aligned} \tag{A6}$$

and take into account that both Y_{lm} and Y^*_{lm} are eigenfunctions of L^2 with eigenvalues $l(l+1)$. From Eq. (A6) it follows that

$$\begin{aligned} \mathbf{L} Y_{l_2 m_2} \cdot \mathbf{L} Y^*_{l_1 m_1} & \\ = \tfrac{1}{2}[L^2 - l_1(l_1+1) - l_2(l_2+1)] Y^*_{l_1 m_1} Y_{l_2 m_2}. & \end{aligned} \tag{A7}$$

After substitution of Eq. (A7) into Eq. (A5) and Eq. (A5) into expression (A1), we finally obtain

$$\begin{aligned} \int \mathrm{d}^3 r \tilde{g}(l_1; r) Y^*_{l_1 m_1}(\mathbf{r})(-\nabla \cdot \delta D \nabla)\tilde{g}(l_2; r) Y_{l_2 m_2}(\mathbf{r}) & \\ = \int \mathrm{d}^3 r \, \delta D \left[\frac{\partial \tilde{g}(l_1; r)}{\partial r} \frac{\partial \tilde{g}(l_2; r)}{\partial r} - \frac{\tilde{g}(l_1; r) \tilde{g}(l_2; r)}{r^2} \right. & \\ \left. \times \frac{L^2 - l_1(l_1+1) - l_2(l_2+1)}{2} \right] Y^*_{l_1 m_1} Y_{l_2 m_2}. & \end{aligned} \tag{A8}$$

ACKNOWLEDGMENT

This research was supported by National Institutes of Health grant P41RR0205. The authors are grateful to P. S. Carney for useful discussions.

Corresponding author Vadim A. Markel can be reached by e-mail at vmarkel@altai.wustl.edu.

*Present address, Department of Bioengineering, University of Pennsylvania, Philadelphia, Pennsylvania 19104 (e-mail: schotland@seas.upenn.edu).

REFERENCES

1. B. Chance, R. R. Alfano, M. Tamura, and E. M. Sevick-Muraca, *Optical Tomography and Spectroscopy of Tissue*, Proc. SPIE **4250**, (2001).
2. *Biomedical Optics*, Vol. 71 of OSA Trends in Optics and Photonics Series (Optical Society of America, Washington, D.C., 2002).
3. V. A. Markel and J. C. Schotland, "The inverse problem in optical diffusion tomography. I. Fourier–Laplace inversion formulas," J. Opt. Soc. Am. A **18**, 1336–1347 (2001).
4. S. R. Arridge, "Optical tomography in medical imaging," Inverse Probl. **15**, R41–R93 (1999).
5. V. A. Markel and J. C. Schotland, "The inverse problem in optical diffusion tomography. II. Inversion with boundary conditions," J. Opt. Soc. Am. A **19**, 558–566 (2002).
6. J. C. Schotland and V. A. Markel, "Inverse scattering with diffusing waves," J. Opt. Soc. Am. A **18**, 2767–2777 (2001).
7. V. A. Markel and J. C. Schotland, "Inverse scattering for the diffusion equation with general boundary conditions," Phys. Rev. E **64**, R035601 (2001).
8. R. Aronson, "Boundary conditions for diffuse light," J. Opt. Soc. Am. A **12**, 2532–2539 (1995).
9. F. Natterer, *The Mathematics of Computerized Tomography* (Wiley, New York, 1986).